Spray coated silver nanowires as transparent electrodes in OPVs for Building Integrated Photovoltaics applications

Z. Ding[1], V. Stoichkov[1], M. Horie[2], E. Brousseau[3], J. Kettle[1*]

1. School of Electronic Engineering, Bangor University, Dean Street, Bangor, Gwynedd, Wales, LL57 1UT, * Contact author; j.kettle@bangor.ac.uk

2 Frontier Research Center on Fundamental and Applied Sciences of Matters, Department of Chemical Engineering, National Tsing-Hua University, 101, Sec. 2, Kuang-Fu Road, Hsin-Chu, 30013 Taiwan

3 School of Engineering, Cardiff University, Queen's buildings, Newport Rd., Cardiff, CF24 3AA

Abstract

The application of spray coated silver nanowires (AgNWs) onto OPVs for building integrated photovoltaics (BIPVs) is demonstrated. By using AgNWs with PEDOT:PSS, a transparent conductive layer was demonstrated on top of an P3HT:PCBM active layer with a sheet resistance of 30Ω/ for 90% transparency. This has been applied to two separate configurations; semi-transparent OPVs for solar glazing applications and OPVs onto an opaque substrate, namely steel. For the latter, a novel technique to planarise the steel substrate with an intermediate layer is also presented, with a substantial decrease in surface roughness reported to ensure that the substrate is smooth enough to use for OPV fabrication. The use of SU-8 as an intermediate layer reduced the surface roughness to R_A = 10nm, which is one of the lowest values reported to date, and was achieved on a low cost substrate (DC01 low carbon steel) using solution processing.

1. Introduction

Building Integrated Photovoltaics (BIPVs) comprises of a group of solar cell technologies that are built into (instead of installed onto) the building structure and can replace some building materials (such as windows or roofs) [1,2]. BIPV's potential to readily integrate into the building envelopes holds aesthetic appeal for architects, builders and property holders. Currently, BIPVs claim a very small share of the PV market, but it is with the emergence of technologies such as organic photovoltaics (OPVs), this proportion could increase [3]. OPV technology does possess numerous advantages over existing solar cell technologies for BIPVs. These include the ability to tune the appearance of the module, low cost of raw materials, low toxicity of materials,low rare metal usage for solar cell construction and low energy payback time [4,5].

Currently, there are two primary BIPV applications sought by users of OPV technology; firstly, semi-transparent OPVs for applications in bus shelters, green houses or solar glazing applications. In the case of a semi-transparent OPV, a transparent substrate of glass or plastic is normally used along with two transparent electrodes [6, 7]. The second application is for roof mounted PVs, where an opaque building material is normally used as the substrate. Today, steel remains one of the primary materials used in many external structures such as industrial storage and commercial buildings for use in roofing and facades. Several groups have demonstrated devices on steel including Galagan et al., who laminated OPVs onto steel substrates [8] and Kumar [9] who used high grade steel as an electrode for OPVs.

To create a truly building-integrated PV, as opposed to a building attached PV, compatibility is needed between the substrate and the solar cell materials and process conditions. For this reason, an intermediate layer (IL) must be coated between the steel and solar cell. In the case of OPVs, the requirements for this layer are very demanding as the active layer needs to be deposited onto a low roughness underlying substrate (typically R_A <20 nm). Therefore, this IL layer must planarise the surface, as well as be an insulator to the steel substrate, which is important for large area monolithic cell integration. Typical ILs are composed of single or multi-layers, using ceramic materials such as SiO_x and Al_2O_3 deposited by vacuum (physical vapour deposition (PVD) and plasma enhanced chemical vapour deposition (PECVD)) or non-vacuum (sol-gel, anodization) techniques [10,11]. To date, the best surface roughness achieved is around R_A = 12 nm using vacuum-deposited radio frequency PVD onto stainless steel substrates [12].

In the case of these BIPV applications, a transparent top electrode is also needed. To achieve this, Galagan et al. used a silver grid electrode and Kumar et al. used a PEDOT:PSS layer. Other potential alternatives which have been reported include graphene [13] and thin metallic layers [14]. Silver nanowires (AgNWs) have also recently emerged as a promising solution to act as transparent electrode for OPVs. This is due to their comparable optical and electrical performance to ITO and have been demonstrated in non-inverted structures [15,16] and inverted structures [17,18]. However, scientific challenges still remain to establish AgNWs as a serious candidate solution due to their processing and high surface roughness leading to electrical shorts.

In this work, we have developed a novel approach to fabricate OPVs onto steel using spray-coated silver nanowires (AgNW) as transparent electrodes. By spray coating, the transparent electrodes possessed a sheet resistance of 30Ω/ at 90% transparency. To enable OPVs on steel, a solution processible approach has also been developed whereby a epoxy IL is coated onto steel. The roughness of this IL is one of the best reported on a steel substrate. Furthermore, this has applied to low carbon steel (DC01), which is a low cost, high roughness steel grade and the demonstration of OPV devices on such a

substrate could provide a route for low cost module fabrication for BIPV applications. The device configuration can also be used for fabrication of semi-transparent OPVs by using a glass substrate. These were used to create semi-transparent OPVs, which produced an average transparency of 51% from 350-800nm.

2. Experimental

2.1 Device fabrication of semi-transparent OPVs

Solar cells on glass substrates composed of a transparent bottom electrode, a thin-film active layer, and a transparent top electrode have been constructed. The schematic in figure 1(a) provides an overview of the device structure and illumination is possible through the top or bottom electrode. These cells were based on indium tin oxide (ITO) coated glass substrates (R_s = 18 Ω/□, transparency=84% with glass, transparency=94% without glass, purchased from Xinyan Ltd.) which were cleaned using deionised water, acetone and isopropanol, then treated in an oxygen plasma for 10 minutes.

On the electrode, an zinc oxide electron transporting layer was prepared from zinc acetate dehydrate (109 mg) dissolved in 2-methoxyethanol (1 ml) and ethanolamine (0.03 ml) solution, which was spin-coated at 2000 rpm on the metal electrode. The samples were then annealed in the presence of atmospheric air at temperatures of 150ºC for 30 minutes so that the zinc acetate to calcinate into zinc oxide [19]. After annealing, the thickness of the ZnO was measured at 30nm using AFM. Active layer blends using poly(3-hexylthiophene) (P3HT) and [6,6]-Phenyl-C_{61}-butyric acid methyl ester (PCBM) with weight ratios 5:4 were prepared and mixed with chlorobenzene solvent with a concentration of 30 mg/mL. Samples were stored in a nitrogen atmosphere glovebox ([O_2], < 1ppm; [H_2O], <100ppm), where the active layers was applied by spin-casting from the 60ºC solution. The active layer were annealed at 140ºC for 60 minute before the hole transport layer i.e. Clevios HTL PEDOT:PSS, was spin-coated at 4000 rpm. The transparent top electrode was fabricated by spray coating of PH1000 PEDOT:PSS (purchased from Ossila) and 0.5 mg/mL silver nanowire (Ag NW) (L-50, purchased from ACS Materials) in ethanol subsequently onto the HTL in fume hood through a shadow mask with an air brush. The PH1000 was modified by dimethyl sulfoxide (DMSO) at different concentration, from 5 vol% to 40 vol% (see detail in next section). Both AgNW and PEDOT mixtures were sonicated for 10 minute before applying.

2.2 Steel preparation

In this work, four grades of steel have been selected for trials. Different types of steels were identified; stainless steel (AISI430), galvanized/aluminized cold rolled low carbon steel (DX51D+Z and

DX51D+AS), uncoated low carbon steel (DC01). AISI430 possessed the lowest initial roughness, but the highest cost, whereas DC01 exhibited the highest roughness and the lowest cost. All the steels were subjected to a high steel speed cold rolled process in order to decrease their thickness to 0.3 mm and roughness at MK Metalfolien GmbH, Hagen, Germany. After rolling, the roughness of the DC01 steel reduced and exhibited the smoothest surface finish (see table 1), although the level of the roughness (R_A =0.10μm, R_{MAX} =0.71μm) was too great to use for OPV fabrication. The substrates were cut to 2x2cm sizes and cleaned by subsequent sonication in DECON, DI water, followed by solvent cleaning using. After cleaning and characterisation, an IL epoxy layer of SU-8 2050 (Chestech ltd., UK) was doctor bladed and spin coated at 2000 rpm onto the cleaned substrate, and cured at 150ºC for 15 minute and then hard baked at 250ºC for 10 minute.

2.3 **Device fabrication of OPVs on steel**

The schematic in figure 1(b) provides a representation of the device structure of a top illuminated OPV, which was fabricated onto a steel substrate. Crucially, an SU-8 IL was deposited, which dramatically reduces the surface roughness of the steel. Aluminium (Al), silver (Ag) or chromium (Cr) electrodes were thermally evaporated onto the epoxy-coated steel substrate through a shadow mask in an Edwards 306 thermal evaporator. After optimisation of the metal electrode, the following layer structure were fabricated for final device testing: steel/SU8/Al/ZnO/P3HT:PCBM/CLEVIOS^{TM} HTL/AgNW. Except for the steel/SU8 and Al, all the other layers were the same as opaque substrate cells.

2.4 Characterisation

For the surface roughness measurement, a map of the surface topography was obtained first using a white light interferometric (WLI) microscope (Micro-XAM from KLA-Tencor, USA). A high-pass filter was applied on the obtained surface maps to remove their waviness components. Additional algorithms provided by the WLI software were utilised in accordance with the BS EN ISO 4287:1998 standard to compute and to average the considered roughness metrics over five sampling lengths for each obtained map of a scanned topography. Scanning Electron Microscopes (SEM) images were also obtained under a field emission gun SEM (Carl Zeiss 1540XB) without specimen coating.

Current density- Voltage (*J-V)* characteristics of these PV devices were measured under white light illumination (AM1.5) using a Newport Class A solar simulator with output intensity of 100 mW/cm^2. The electrical performance of the devices was measured with a SMU connected to a BNC electrical probe. An aperture mask was used to ensure accurate active layer area illumination. All devices used in this work had an active area of 1 cm^2.

3. Results and Discussion

3.1 Semi-transparent OPVs with AgNW electrodes

The schematic in figure 1(a) provides an overview of the device structure for semi-transparent OPVs. In this work, a composite electrode consisting of Clevios PH1000 (PEDOT:PSS) and AgNWs was used as the top electrode. Both material can be spray coated in ambient using an environmentally safe solvent e.g. ethanol or water. On its own, PH1000 proved too resistive for higher performing devices leading to parasitic resistances in the device. Therefore, films of PH1000 were deposited by spray coating with various concentrations of DMSO as segregation promotion additive [20,21], as shown in Figure 2. By steadily increasing the DMSO content to an optimum of 10%, a significant improvement in sheet resistance (R_{SH}) i.e. ~40 Ω/ for 57% transparency and ~300 Ω/ for 80% transparency was achieved. Further increase in DMSO content resulted in no conductivity gains and a prolonged film drying time, leading to uneven thickness distribution, so an optimal DMSO content of 10% was selected. DMSO is needed to ensure highly conductive layers of PEDOT:PSS are deposited. However, due to the high boiling point of DMSO, trace amounts of DMSO is very likely to remain after coating of the PEDOT:PSS. It known that these additives can influence the long term stability of the OPV, however, DMSO has been shown to be the most stable additive for this configuration [21].

To see the impact of using only Clevios PH1000 with DMSO as the anode, P3HT:PCBM cells were fabricated onto ITO glass substrate (ITO/ZnO/P3HT:PCBM/CLEVIOS^{TM} PEDOT HTL/PH1000) and benchmarked against a standard inverted OPV device with an evaporated top electrode cell (ITO/ZnO/P3HT:PCBM/CLEVIOS^{TM} PEDOT HTL/Ag). Figure 4(a) and the table 1 show the performance of the cells. As the solar cell is bifacial, it can be illuminated from either the ITO side or the PH1000 side. An optimised PCE of 0.9% was achieved under AM 1.5 G solar simulator measured from the PH1000 side, whilst 1.9% were achieved when measured from the ITO side. In addition, the fill factor (FF) of the PH1000 device was much lower than that of the reference cell, indicating that the conductivity of PH1000 was leading to resistive losses. The size of the devices in this work was 1 cm^2 and larger areas are likely to lead to even greater resistive losses.

Therefore, spray coated AgNWs were applied to improve the conductivity of the anode. The electrical and optical properties of the AgNW layer are closely related to the amount of AgNW deposited. Increasing the content of silver deposited by spray coating reduces the sheet resistance of the transparent top electrode because the inter-connectivity of the AgNW network is greater. However , this has a

negative impact on the optical transmittance due to optical reflection [16]. The optimised spray coating process gave sheet resistance of 30Ω/□ for 90% transparency (as shown in figure 3), this was close to that of ITO on glass substrate (Figure 3). However, when the AgNW was applied directly onto the spin-coated CLEVIOS^{TM} HTL PEDOT:PSS, the spin-coated ultra-thin PEDOT layer (thickness < 20 nm) detached from the active layer due to solvent dewetting. This lead to poor cell performance due to appearance of s-shaped IV curves. However, by applying a relatively thick PH1000 PEDOT:PSS layer (thickness ≈70 nm) on to the HTL PEDOT:PSS prior to AgNW spray coating, there was no dewetting. As the solar cell is bifacial, it can be illuminated from either the ITO side or the AgNW side. After optimising this hybrid transparent electrode, the PCE of ITO substrate cell improved to 1.5%, when measured from the AgNW side. This is still lower than the performance measured from the ITO side, 2.1% (Figure 4 (b) and table 1) and is primarily due to the increased absorption originating from the thicker PEDOT:PSS layer. If the thickness could be reduced, a 10-15% relative improvement could be achieved [22].

Whilst the performance is somewhat lower than the reference cell, which has an opaque, metallic anode, the device exhibits similar performance to other semi-transparent devices and is demonstrated over a relatively larger area (1 cm^2). The low R_{SH} of the anode should ensure scalability to larger areas. Overall the transparency of the device was measured at 51% between the wavelengths of 350-800nm (see SI-1).

3.2 Intermediate layer (IL) deposition for OPVs on steel

From our studies using steel substrates, OPV performance is sensitive to surface roughness and any high roughness structures over the dimensions of the substrate must be avoided. Therefore to integrate into opaque substrates such as steel, substrate roughness in the nanometer range is required to provide a surface that will promote high-quality deposition of subsequent layers and prevent the penetration of potential substrate irregularities into the organic layers, which could lead to electrical shorts. From our experimental work, surface roughness (R_A) greater than 30 nm leads to a significant drop in performance (see SI-2).

Shown in figure 4 is the surface topography of the samples prior to IL layer deposition from WLI measurements of a) AISI430, b) DX51D+Z, c) DX51D+AS and d) DC01with a summary shown in Table 2. A permanent epoxy layer (SU8-2050) was used in this work for IL deposition and the result of the coating is shown in figure 4 for e) AISI430, f) DX51D+Z, g) DX51D+AS and h) DC01. Table 2 summarizes the data with the surface roughness measurements after cleaning. It is clear that the SU8 IL reduces the surface roughness down to an acceptable value of R_A = 10 nm, making it viable for integration into an OPV module, with the film thickness measured at 30 µm. It can also be stated that irrespective of the steel grade, the final roughness is almost identical. This is significant as normally stainless steel is used for PV substrates due to the lower initial surface roughness. To produce steel sheets suitable for PVs,

a cold rolling process is always needed. In the case of stainless steel (AISI430), it is estimated the costs is £2680/ton (3300 €/ton) for 0.3 mm thickness, whereas for DC01, the cost is £1390/ton (1800 €/ton) for the same 0.3mm thickness. Therefore, the processing route proposed in this paper sets out an alternative strategy to integrate steel into PV production using much lower cost steel substrates than reported before [23]. The remainder of this article focuses on using DC01 steel. Whilst DC01 provides a lower cost substrate, further studies should be undertaken comparing the stability of DC01 to the other steel grades to compare the long-term stability, as impurities from the steel could diffuse into the OPV substrate.

3.3 OPVs made onto steel with AgNW electrodes

Manufacturing OPVs onto opaque substrate such as steel inherently has a number of issues. Firstly, when fabricating on opaque substrates, a lower cost metal electrode should be used rather than ITO. However, this could lead to interfacial issues. For example surface oxidation of metal could alter the surface work function, thus OPV performance. In this work we investigated several metallic materials, including silver, aluminium and chromium-coated aluminium in comparison of ITO. These metal electrodes were thermally evaporated on glass substrate via a shadow mask and were then made into diodes with conventional inverted cells' structure i.e. Metal electrode/ZnO/P3HT:PCBM/PEDOT/Ag. As a variety of electrode materials (including alloys) and configurations were tested, a method to evaluate the suitability of the electrodes in devices. This consisted of a simple diode I-V characteristics in dark conditions, with measurements of the number of working diodes (i.e. 'diode yield') noted. A high diode yield indicated good rectification, no electrical shorts or open circuit. Using ITO as the Metal electrode, a 100% diode yield was obtained. In contrast, thermally evaporated silver (Ag) electrode showed only 27.7% diode yield. In spite of the fact that the roughness of thermally evaporated Ag was only few nanometers and was lower than the ZnO deposited on top, most devices were leaky. The origin of this leakage appears to be metallic diffusion or mixing of the bottom electrode into the active area during the processing. Therefore, thermally evaporated Al electrodes were trialled instead. Bare Al electrode had diode yield of 66.7%, with the remaining 33.3% cells showed no diode behaviour, i.e. open circuit. This is likely to be due to surface oxidation of Al. However, by adding a protective Cr layer of ≈3 nm, diode yield increased to 100%, the same as ITO. Both Al electrode and Cr-coated Al electrode were used to make solar cells. All working cells with Al bottom electrode showed obvious S-shape on their *J-V* curves likely due to a potential barrier or dipole from the surface oxidation layer. The Cr coated Al, as opposed to bare Al, showed IV curves closer to the ideal characteristics and devoid of the S-shape.

The second problem was due to the hydrophobic nature of the active layer, so coating PEDOT:PSS directly onto the active layer led to de-wetting and a non-uniform layer. This is in agreement

with observations by Wilken et al. [24], who reduced this effect by dispersing the PEDOT:PSS in alcohols. In our work, we utilised CLEVIOS^{TM} HTL Solar PEDOT:PSS which has previously been demonstrated as spin-coatable hole transporting layer [25] onto hydrophobic active layer for OPVs. Based on this layer, other hydrophilic material or evaporated metal layers could be applied to the surface. By using the CLEVIOS^{TM} HTL, the original de-wetting problem was eliminated.

Thirdly, and most importantly, most OPVs use either an anode or a cathode that contains a metal oxide transparent conducting oxide (TCO) to act as a contact, such as ITO or FTO. Deposition of such material requires vacuum and high temperature, which is expensive and can cause substrate damage as a result of either UV-exposure from the plasma, heating up of the active layers, or damage to the polymer films by high energy ions. This, in the scenario of opaque substrate solar cells, where the transparent layer are on top of active layer and charge transport layers, could be detrimental for the performance. As a result, the same composite electrode system as section 3.1 was used.

Based upon this optimised structure, an OPV device area of 1 cm^2 was fabricated onto DC01 steel planarised using SU-8. Figure 6 shows optical images of the significant layers surfaces which are applied sequentially during the OPV fabrication. In Figure 5(a), an optical image of the DC01 steel substrate is shown, which corroborates the WLI data indicating the relative high roughness of the underlying substrate. In Figure 5(b), the surface of the active layer after annealing is shown and the surface is observed to be flat, uniform and free of defects. On top of the active layer, the PEDOT:PSS layer is deposited [figure 5(c)]. The layer is clearly not as uniform and this is likely to be due to dewetting or non-uniform solvent evaporation. Finally, figure 5(d) shows the top surface consisting of the spray coated AgNWs; the high interconnectivity of the AgNWs supports the measurements of low sheet resistance.

A PCE of 2.3% was achieved with our optimised process (figure 4 (c) and table 1), with the short-circuit current (J_{SC}) measured at 8.2 mA cm^{-2}, open-circuit voltage (V_{OC}) at 0.53, and FF at 0.53. By comparison a control device of ITO-glass exhibits PCE = 3.0 %, V_{OC} = 0.55 V, J_{SC} = 9.4 mA cm^{-2}, and FF = 0.57. This was 23% lower than the PCE of an OPV made onto a glass substrate with the same active layer material (see table 1 – bottom-top electrode is ITO-Ag). The decrease in J_{SC} is primarily due to increased absorption in the PH1000 layer, indicating that improvements could be achieved with a thinner layer, if the dewetting issues can be prevented. In the case of the control device, the light transmittance through the glass-ITO-ZnO layer is very high (92%), which correlates to the higher J_{SC}. The slightly lower FF for the device is a due to low shunt resistance observable in the *J–V* at zero bias. SEM imaging was used to evaluate the device and is shown figure 5 (a), which reveals that the interconnection between Ag NW and the preceding PH1000 layer was reasonably good. Figure 5(b) shows that the distribution and the interconnection of AgNW on the cells surface was also satisfactory. Therefore, the

performance decreases is likely to be due to shorting pathways across the thin semiconductor active layers as a result of non-perfect planarization.

Finally, considerations for commercialization should be made. Based upon the steel thicknesses used in this paper (0.3mm), the cost of the steel substrate is 3.2 Euro per m^2 for DC01. This includes the costs of cold rolling to thin and initially smooth the steel substrates. Considering our current SU8 material usage and cost to purchase, the final substrate cost is estimated at 29 Euro per m^2. Whilst this is more expensive than other polymeric substrates, steel offers potential of integration directly into built-environment i.e. roof cladding. It is also important to consider the long-term stability and particular the differences in the coefficient of thermal expansion (CTE). For P3HT:PCBM, the CTE is around 6×10^{-4} m/m K^{-1} [26]. For bare carbon steel, the CTE is 1×10^{-5} m/m K^{-1}[23]. Initial thermal cycling under ISOS-T-2 tests show a 19% relative decrease in PCE after 100 cycles (See SI-4). Further environmental testing is needed to understand the impact of this difference until a final product is complete.

4. Conclusions

In conclusion, we demonstrated a novel process that can be used to make OPVs onto opaque substrates or for semi-transparent devices using AgNW transparent electrodes. A hybrid transparent conductive layer which utilised PH1000 PEDOT:PSS and AgNW was used as the top electrode in both cases, which demonstrated a sheet resistance of 30Ω/□ for 90% transparency. When applied to semi-transparent OPVs, a PCE of 2.1% was achieved. In addition, a novel technique to planarise steel was presented, with substantial decreases in roughness reported to ensure that the substrate is smooth enough to use for OPV fabrication. The use of SU-8 as an intermediate layer reduced the surface roughness to R_A = 10nm, which is one of the lowest values reported to date, and was achieved on a low cost substrate (DC01 low carbon steel) using solution processing. Using the DC01 steel substrate, OPV were successfully made solar cell with PCE of 2.3% over an area of 0.8 cm^2. The reported approach can be readily transferred to other grades of steel. This provides some confidence that it could be adopted in other types of opaque building materials such as slate, shingles, ceramic tiles or metal cladding, providing that the intermediate layer coating step is undertaken.

Acknowledgements

We would like to acknowledge the support of the John Bayley of H.C. Starck Clevios GmbH in Leverkusen for advice on PEDOT:PSS deposition. In addition, the support of Yun Lan of MK Metallfolien Gmbh, Hagen is gratefully acknowledged. Last but not least, the authors would like to thank Dr Pascal Sanchez, Dr David Gomez and María Fe Menéndez of Fundacion ITMA, Aviles, Spain, for

advice on nanowire deposition. The research leading to these results has received funding from the European Union's Research Fund for Coal and Steel (RFCS) research programme under grant agreement nº RFSR-CT-2014-00014

Table 1. The performance of solar cell on ITO glass substrate with PH1000 as top anode; ITO glass substrate with Ag NW as top electrode and Al coated planarized steel substrate with Ag NW as top anode.

Substrate	**Bottom-Top Electrode**	**Jsc (mA/cm^2)**	**Voc (V)**	**FF**	**PCE(%)**	**Corresponding I-V graph**
Glass	ITO-Ag	9.4	0.55	0.57	3.0	Not shown
Glass	ITO-PH1000	4.1 (8.29)	0.55 (0.59)	0.38 (0.38)	0.9 (1.9)	3(a)
Glass	ITO-Ag NW	(8.3)	0.53 (0.52)	0.42 (0.49)	1.5 (2.1)	3(b)
Low carbon steel (DC01)	Al/Cr-Ag NW	8.2	0.53	0.53	2.3	3(c)

Note: Value in brackets were illuminated from ITO glass side, otherwise were from transparent top electrode side.

Table 2. Measure surface roughness of steel grades made using WLI, before and after coated with the SU-8 intermediate layer (IL). After coating with SU-8, the roughness is reduced to a level that is enables OPVs to be readily fabricated onto

	AISI430		DX51D+Z		DX51D+AS		DC01	
	No coating	With SU-8	No coating	With SU-8	No coating	With SU-8	No coating	With SU-8
R_A (μm)	0.10	0.012	0.097	0.015	0.083	0.010	0.083	0.010
R_Q (μm)	0.13	0.015	0.12	0.018	0.10	0.012	0.10	0.012
R_{MAX} (μm)	0.71	0.063	0.63	0.057	0.51	0.055	0.59	0.049

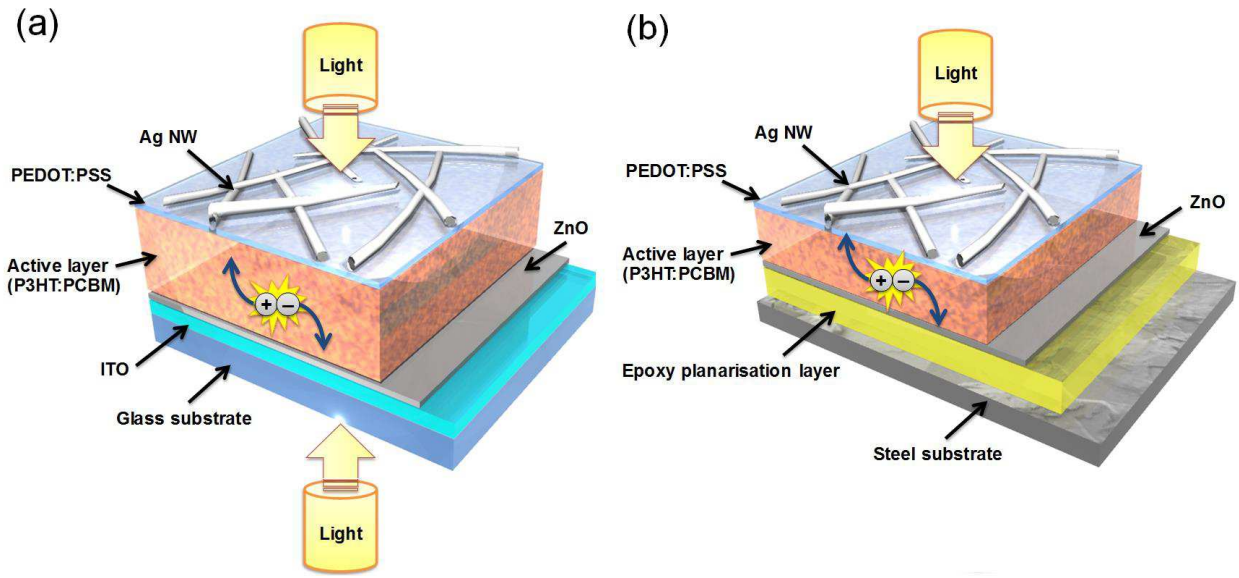

Figure 1: Schematic of the (a) semi-transparent OPV where photocurrent can be achieved bifacially and (b) of the OPV manufactured onto steel. Planarization of the underlying substrate is imperative to ensure no electrical shorts are present.

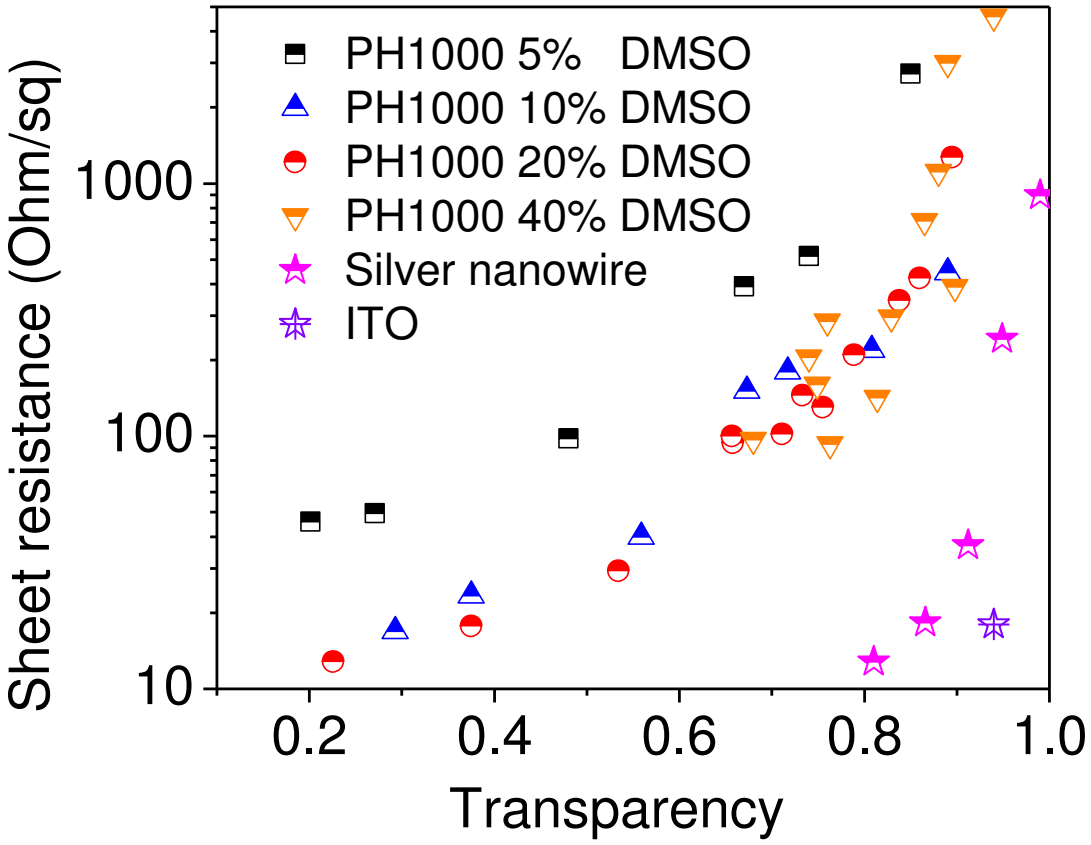

Figure 2: Sheet resistance versus transparency of PH1000 (with various amount of DMSO additive with their volume percentage shown in the figure); Ag NW sprayed on glass slides and ITO. The absorption of glass substrate was excluded from the result.

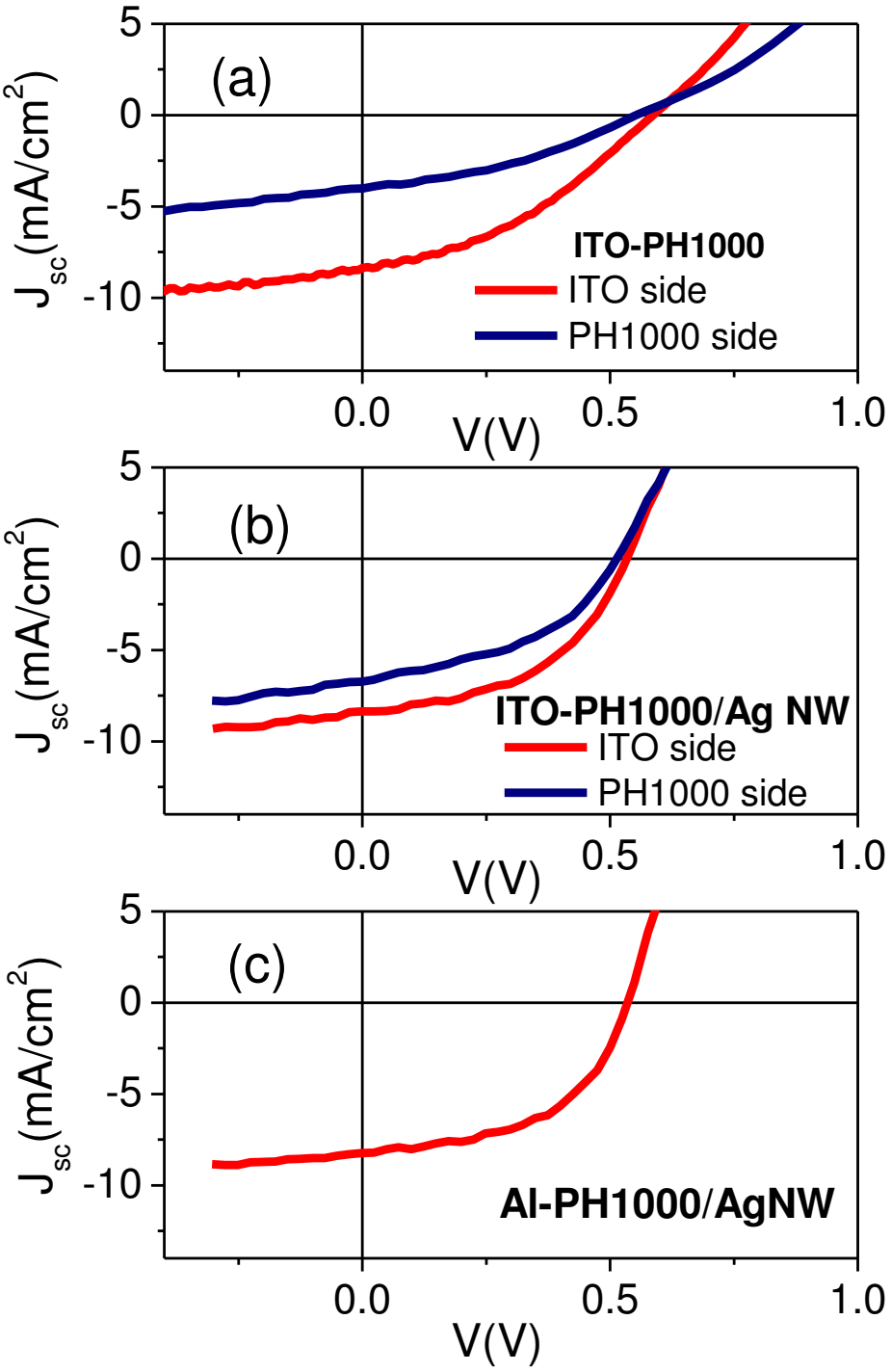

Figure 3: *J-V* curves of solar cell on a) ITO glass substrate with PH1000 PEDOT:PSS top electrode; b) ITO glass substrate with PH1000/Ag NW top electrode; c) planarized steel substrate with Al/Cr bottom electrode and PH1000/Ag NW top electrode. Performance parameters are summarised in table 1. In figure a) and b), as the OPV is bifacial, measurements were conducted from both the ITO side and the AgNW side (see figure 1(a) for a schematic)

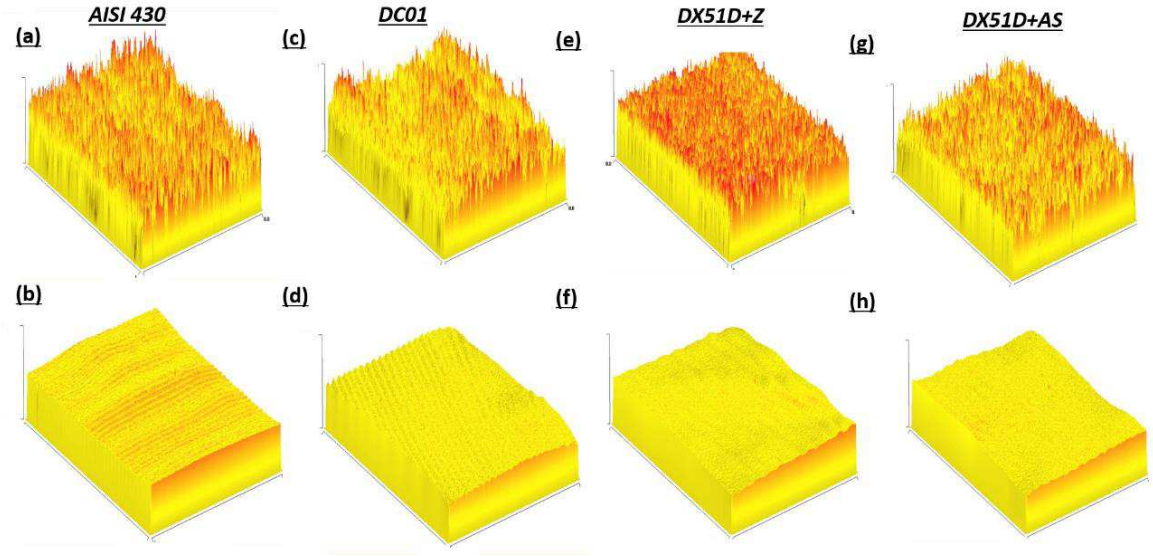

Figure 4: White light interferometry measurements over 6mm areas of (a) AISI430 before and (b) after application of SU-8 IL, (c) DC01 before and (d) after application of SU-8 IL, (e) DX51D+Z before and (b) after application of SU-8 IL and (f) DX51D+AS before and (b) after application of SU-8 IL. The area size all each measurement is 6x8mm (x and y axis, respectively), with a z-axis range between 0-100um

Figure 5:

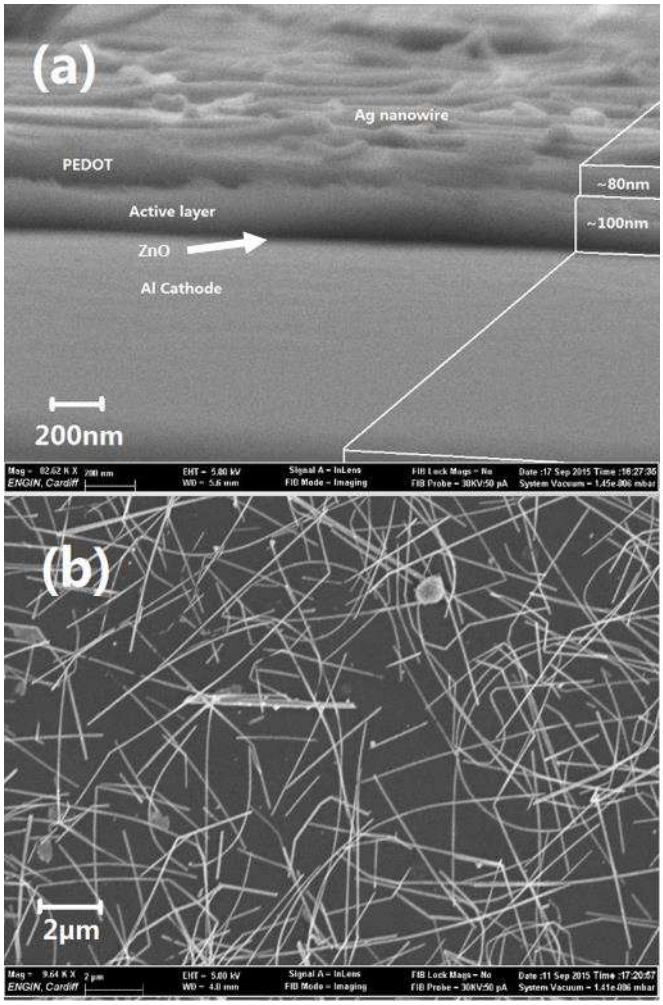

Figure 5: SEM cross section (a) and top surface (b) of solar cell with configuration of Al/Cr/ZnO/P3HT:PCBM/PEDOT HTL/PH1000/Ag NW

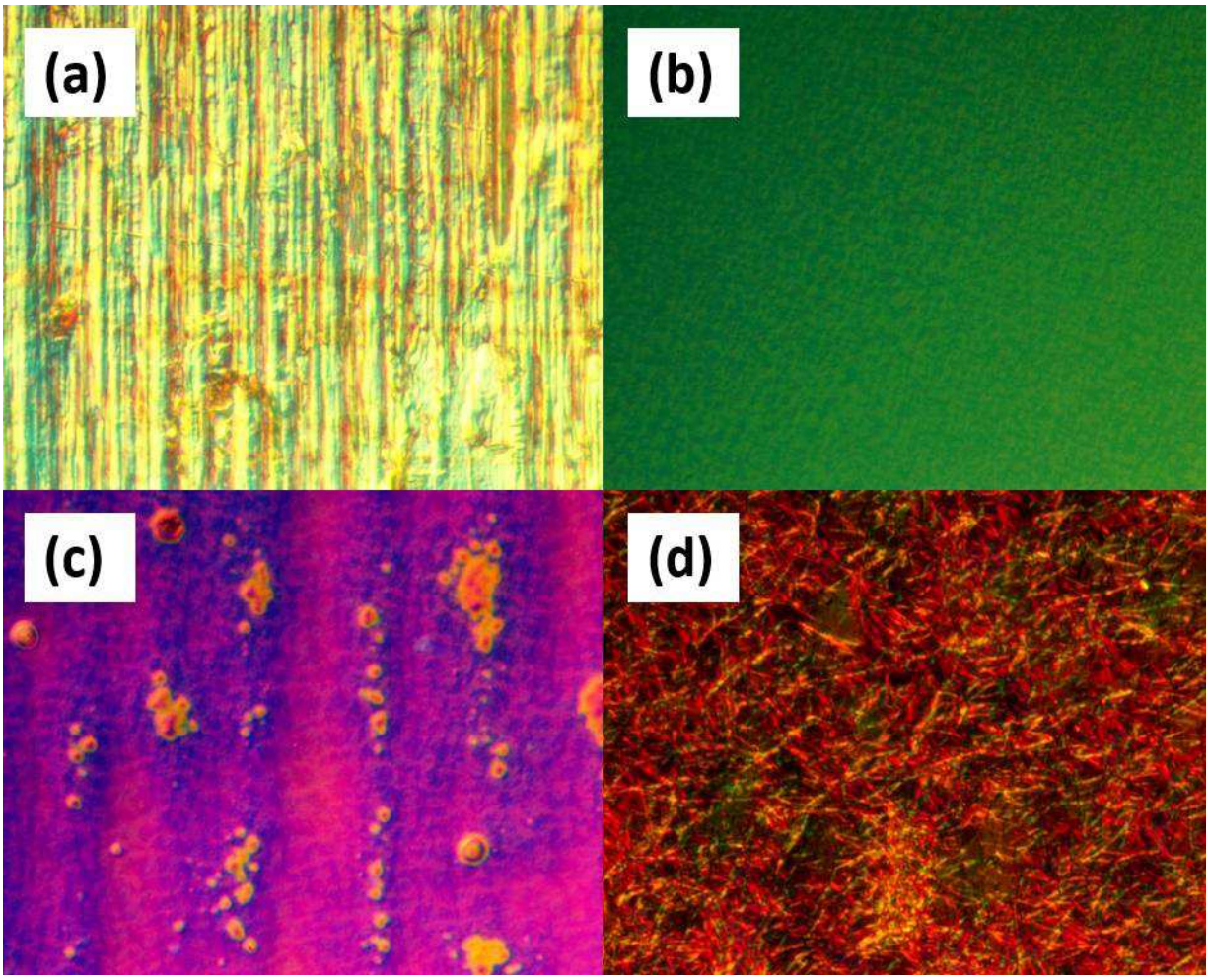

Figure 5: Optical microscope images (taken at 20x magnification) showing the surface of (a) the DC01 steel substrate, (b) the P3HT:PCBM active layer (c) PEDOT:PSS layer and (d) AgNW top electrode

References

[1] B. P. Jelle, C. Breivik, H.D. Røkenes, Building integrated photovoltaic products: A state-of-the-art review and future research opportunities, Solar Energy Materials and Solar Cells, 100 (2012) 69-96.

[2] V. Shrotriya, Organic photovoltaics: Polymer power, Nature Photonics, 3(8) (2009) 447-449.

[3] G.P. Hammond, H.A. Harajli, C.I. Jones, A.B. Winnett, Whole systems appraisal of a UK Building Integrated Photovoltaic (BIPV) system: energy, environmental, and economic evaluations. Energy Policy, 40 (2012) 219-230.

[4] Y. S. Zimmermann, A. Schäffer, C. Hugi, K. Fent, P.F.X. Corvini, M. Lenz, Organic photovoltaics: Potential fate and effects in the environment. Environment International, 49 (2012) 128-140.

[5] M. C. Scharber, D. Mühlbacher, M. Koppe, P. Denk, C. Waldauf, A.J. Heeger, C.J. Brabec, Design rules for donors in bulk-heterojunction solar cells—Towards 10% energy-conversion efficiency. Advanced Materials, 18(6) (2006) 789-794.

[6] F. Yan, J. Noble, J. Peltola, S. Wicks, S. Balasubramanian, Semitransparent OPV modules pass environmental chamber test requirements. Solar Energy Materials and Solar Cells, 114 (2013) 214-218.

[7] K. S. Chen, J. F. Salinas, H. L. Yip, L. Huo, J. Hou, A.K.Y. Jen, Semi-transparent polymer solar cells with 6% PCE, 25% average visible transmittance and a color rendering index close to 100 for power generating window applications. Energy & Environmental Science, 5(11) (2012) 9551-9557.

[8] Y. Galagan, D.C. Hermes, P.W. Blom, R. Andriessen, Large area ITO-free organic solar cells on steel substrate. Organic Electronics,13(12) (2012) 3310-3314.

[9] V. Kumar, H. Wang, Selection of metal substrates for completely solution-processed inverted organic photovoltaic devices. Solar Energy Materials and Solar Cells, 113 (2013) 179-185.

[10] T. Yagioka, T. Nakada, Cd-free flexible Cu (In, Ga) Se2 thin film solar cells with ZnS (O, OH) buffer layers on Ti foils. Applied physics express, 2(7) (2009) 072201.

[11] A. L. Martínez, A. Menéndez, P. Sánchez, L.J. Andrés, M.F. Menéndez, J. Izard, D. Gómez, Solar photovoltaic technology on rough low carbon steel substrates for building integrated photovoltaics: A complete fabrication sequence. Solar Energy, 124 (2016) 216-226.

[12] R. Wuerz, A. Eicke, M. Frankenfeld, F. Kessler, M. Powalla, P. Rogin, O. Yazdani-Assl, CIGS thin-film solar cells on steel substrates. Thin Solid Films, 517(7) (2009) 2415-2418.

[13] H. Park, J.A. Rowehl, K.K. Kim, V. Bulovic, J. Kong, Doped graphene electrodes for organic solar cells. Nanotechnology, 21(50) (2010) 505204.

[14] H.M. Stec, R.J. Williams, T.S. Jones, R.A. Hatton, Ultrathin Transparent Au Electrodes for Organic Photovoltaics Fabricated Using a Mixed Mono-Molecular Nucleation Layer. Advanced Functional Materials, 21(9) (2011) 1709-1716.

[15] L. Yang, T. Zhang, H. Zhou, S.C. Price, B.J. Wiley, W. You, Solution-processed flexible polymer solar cells with silver nanowire electrodes. ACS applied materials & interfaces, 3(10) (2011) 4075-4084.

[16] L.J. Andrés, M.F. Menéndez, D. Gómez, A.L. Martínez, N. Bristow, J. Kettle, B. Ruiz, Rapid synthesis of ultra-long silver nanowires for tailor-made transparent conductive electrodes: proof of concept in organic solar cells. Nanotechnology, 26(26) (2015) 265201.

[17] D. Angmo, T.R. Andersen, J.J. Bentzen, M. Helgesen, R.R. Søndergaard, M. Jørgensen, J.E. Carlé,.E.M. Bundgaard, F.C. Krebs, Roll-to-Roll Printed Silver Nanowire Semitransparent Electrodes for Fully Ambient Solution-Processed Tandem Polymer Solar Cells. Advanced Functional Materials, 25(28), (2015) 4539-4547.

[18] J. Ajuria, I. Ugarte, W. Cambarau, I. Etxebarria, R. Tena-Zaera, R. Pacios, Insights on the working principles of flexible and efficient ITO-free organic solar cells based on solution processed Ag nanowire electrodes. Solar Energy Materials and Solar Cells, 102 (2012) 148-152.

[19] J. Huang, Z. Yin, Q. Zheng, Applications of ZnO in organic and hybrid solar cells. Energy & Environmental Science, 4(10), (2011) pp.3861-3877.

[20] C.S. Sangeeth, M. Jaiswal, R. Menon, Correlation of morphology and charge transport in poly (3, 4-ethylenedioxythiophene)–polystyrenesulfonic acid (PEDOT–PSS) films. Journal of Physics: Condensed Matter, 21(7) (2009) 072101.

[21] B. Roth, G.A. dos Reis Benatto, M. Corazza, R.R. Søndergaard, S.A. Gevorgyan, M. Jørgensen, F.C. Krebs, The Critical Choice of PEDOT: PSS Additives for Long Term Stability of Roll-to-Roll Processed OPVs. Advanced Energy Materials, 5(9) (2015) 1401912

[22] J. Kettle, H. Waters, M Horie, S.W. Chang, Effect of hole transporting layers on the performance of PCPDTBT: PCBM organic solar cells, Journal of Physics D: Applied Physics, (2012), 45(12), 125102.

[23] Private communication, Dr Yun Lan, MKM Metallfolien GmbH

[24] S. Wilken, T. Hoffmann, E. Von Hauff, H. Borchert, J. Parisi, ITO-free inverted polymer/fullerene solar cells: Interface effects and comparison of different semi-transparent front contacts. Solar Energy Materials and Solar Cells, 96 (2012) 141-147.

[25] W. Lövenich, PEDOT-properties and applications. Polymer Science Series C, 56(1) (2014) 135-143.

[26] T. Agostinelli, S. Lilliu, J.G. Labram, M. Campoy-Quiles, M. Hampton, E. Pires, J. Rawle, O. Bikondoa, D.D. Bradley, T.D., Anthopoulos, J. and Nelson, Real-Time Investigation of Crystallization and Phase-Segregation Dynamics in P3HT: PCBM Solar Cells During Thermal Annealing. Advanced Functional Materials, (2011), 21(9), pp.1701-1708.